

Supplementary material of the paper “Surface grain-size mapping of braided channels from SfM photogrammetry”

Loïs Ribet¹, Frédéric Liébault¹, Laurent Borgniet², Michaël Deschâtres¹, Gabriel Melun³

1. Université Grenoble Alpes, INRAE, CNRS, IRD, Grenoble INP, IGE, 38000 Grenoble, France

5 2. Université Grenoble Alpes, INRAE, LESSEM, 38000 Grenoble, France

3. Office Français de la Biodiversité, 94080 Vincennes, France

Correspondence to: Loïs Ribet (lois.ribet@inrae.fr)

SfM workflow for image processing with Agisoft Metashape

- 10 The photogrammetric workflow was built following recommendations available in the literature (Eltner et al., 2016; James et al., 2020; Over et al. 2021). It was developed with the primary objective to improve the quality of the outputs, while reducing the computation time as a secondary objective.

1. Sparse points cloud creation

- The first process was the Alignment of the photos. It searches for unique 2D features of high contrast or texture, called *key points*, in each image and matching them across images pairwise into *tie points*. The process finds the position of each *tie point* relative to the camera by aerial triangulation. *Accuracy* was set *High*. It is the best fit considering that the *Highest* setting shuts down the software and the lower accuracies do not use the full resolution of the photos to make the process faster. The Key point limit was set to 400 000 which is a good compromise between time processing and computing enough *key points* considering the performance of the computer. Over et al. (2021) pointed out that “a high limit or unlimited value will likely create more points, but the additional points may be of lower quality”. Since the goal is to compute the roughness on CloudCompare, it was decided to get as much points as we can. Low quality points have been removed with Error reduction tools after. Tie point limit was set to 0 to get the best alignment. Finally, as no lens calibration was provided, *Adaptive camera model fitting* was used.
- 15
20

- Poor geometry *tie points* were removed using the Reduction uncertainty from the Error reduction tool. This step fixes the potential issue caused by setting the preceding Key point limit. Removal of these points does not affect the accuracy of optimization but reduces the noise in the point cloud and prevents points with a large uncertainty in the z-axis from influencing other points with good geometry or being incorrectly removed in the reprojection error step. In Over et al. (2021) the threshold considered for this process was 50 %. However, it was considered here to suppress too much points given that roughness will be computed. A 25 % threshold was thus used.
- 25

- 30 An Optimize camera process was done to re-align the cameras after the points removal. The $b1$ and $b2$ (affinity and nonorthogonality coefficients) distortion parameters were not used.
- Another Error reduction process was done using the Projection accuracy. This tool removes bad points that the software is the least confident about from the sparse cloud due to pixel matching errors during the alignment process. A recommended 50 % threshold was used (Over et al. 2021).
- 35 Considering the high quality of the photos, *tie point accuracy* in the Reference settings was lowered to 0.1 pxl to get a better error reduction from the last Optimize camera.
- A final Optimize camera was done before putting the Ground Control Points (GCPs) by checking the 10 distortion parameters.

2. Ground Control Points

- 40 Once markers were placed on photos, an Optimize camera process was done with the 10 distortion parameters checked. An Error reduction by Reprojection error was performed to filter 10 % of points. A final Optimize camera was performed with the 10 distortion parameters checked.

3. Dense points cloud creation

- The process to Build the Dense points cloud was as such: *Quality* was set *High* and *Depth filtering* was set *Mild*. This last
- 45 setting is preferable when there are many small details which are spatially distinguished in the scene to be reconstructed and thus for important features to not be sorted out as outliers. *Mild depth filtering* mode is also required for the Depth maps based on Mesh reconstruction.

Study sites	Error for the z coordinate of the camera			RMSE of residual errors (m)		
	Mean error (m)	Mean absolute error (m)	Standard deviation of error (m)	Control points		
				Check points		
				X	Y	Z
Arigéol	0.0028	0.0986	0.0129	0.057	0.027	0.013
				0.053	0.032	0.025
Asse	0.0001	0.0190	0.0249	0.055	0.077	0.098
				0.053	0.087	0.108
Béoux	0.0016	0.0213	0.0263	0.052	0.047	0.022
				0.057	0.052	0.031
Bès	-0.0036	0.0213	0.0276	0.044	0.042	0.043
				0.041	0.046	0.055
Bouinenc	0.0002	0.0098	0.0125	0.036	0.032	0.008
				0.021	0.023	0.023
Drac	-0.0011	0.0713	0.0460	0.067	0.069	0.179
				0.066	0.059	0.162
Drôme	-0.0057	0.0133	0.0170	0.066	0.089	0.262
				0.068	0.078	0.364
Ebron	-0.0580	0.0840	0.0141	0.294	0.244	0.047
				0.370	0.276	0.215
Eygues	-0.0568	0.0436	0.0298	0.025	0.171	0.063
				0.024	0.134	0.082
Galabre	0.0010	0.0112	0.0098	0.049	0.039	0.012
				0.034	0.035	0.020
Séveraisse	0.0001	0.0056	0.0118	0.061	0.030	0.015
				0.046	0.029	0.019
St-Pierre upstream	na	na	na	0.054	0.156	0.020
				0.041	0.086	0.018
St-Pierre downstream	na	na	na	0.065	0.062	0.019
				0.143	0.028	0.045

50 Table S1: Error metrics from SfM dense point clouds

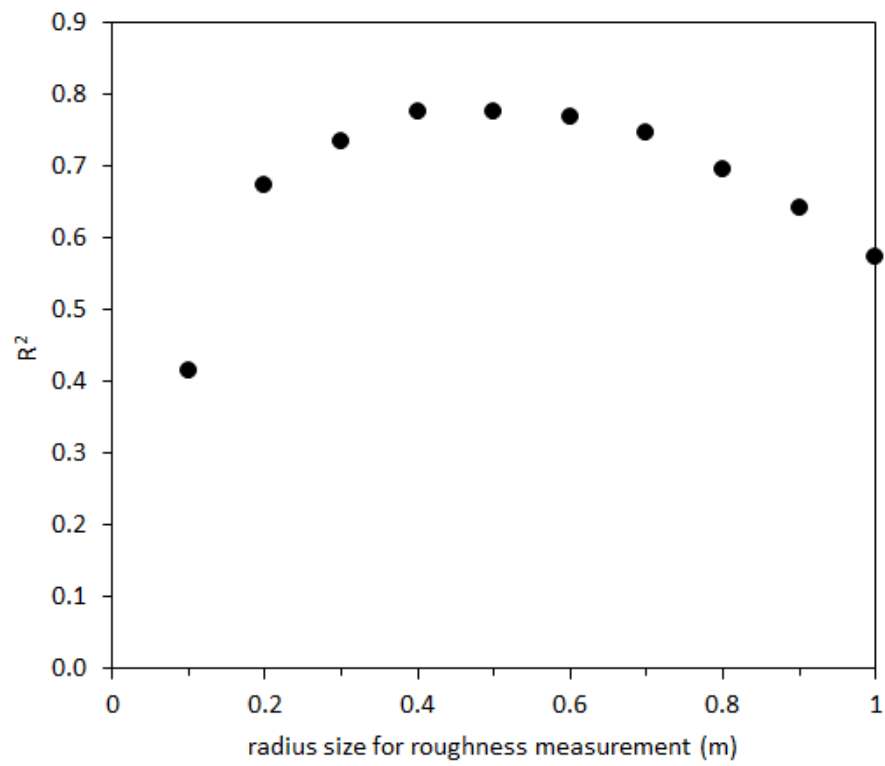


Figure S1: Sensitivity analysis for the determination of the optimum radius used to compute roughness predictors. Optimum range is comprised between 0.4 and 0.5 m, according to the R^2 of the $D_{50} \sim R_h$ regression analysis.

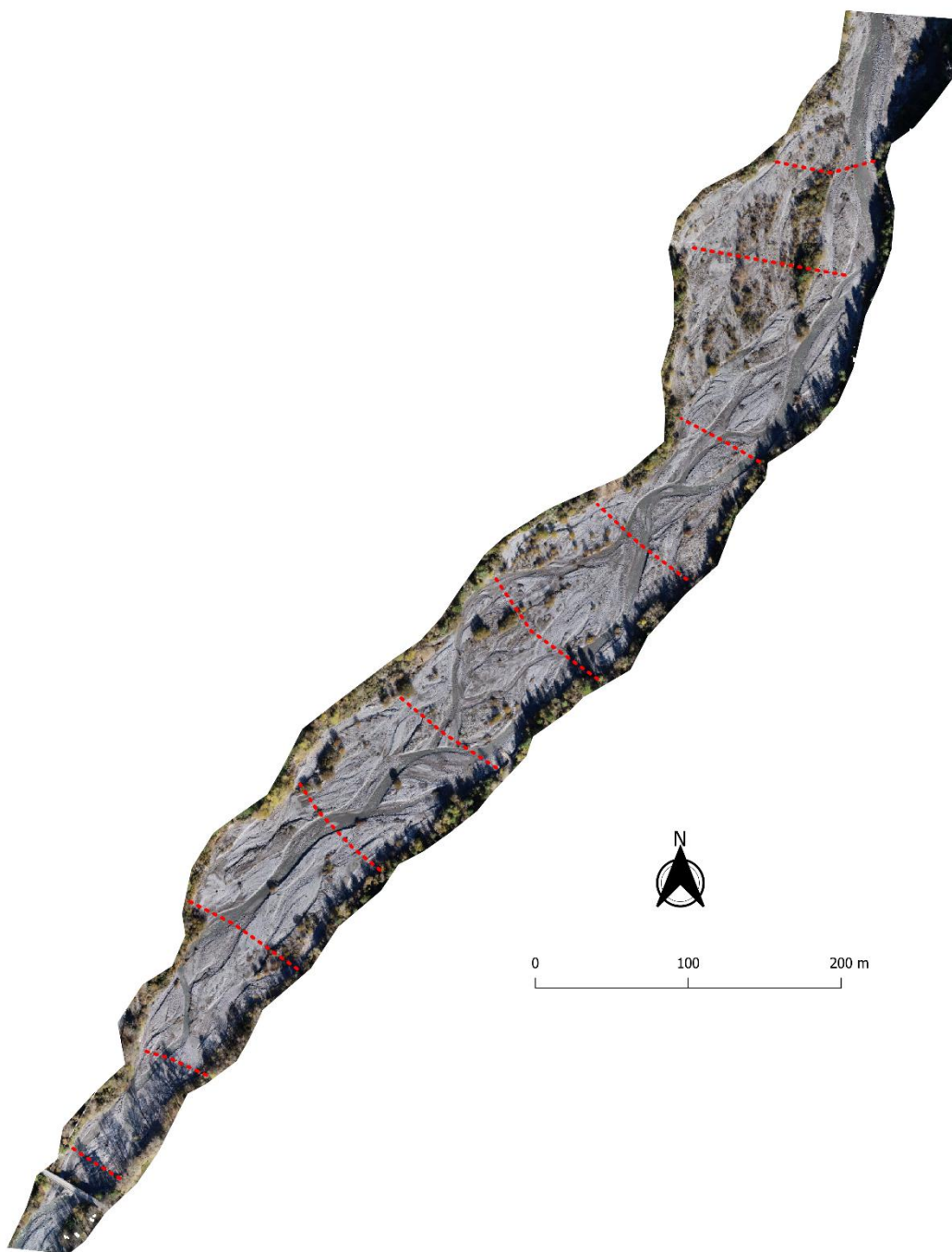
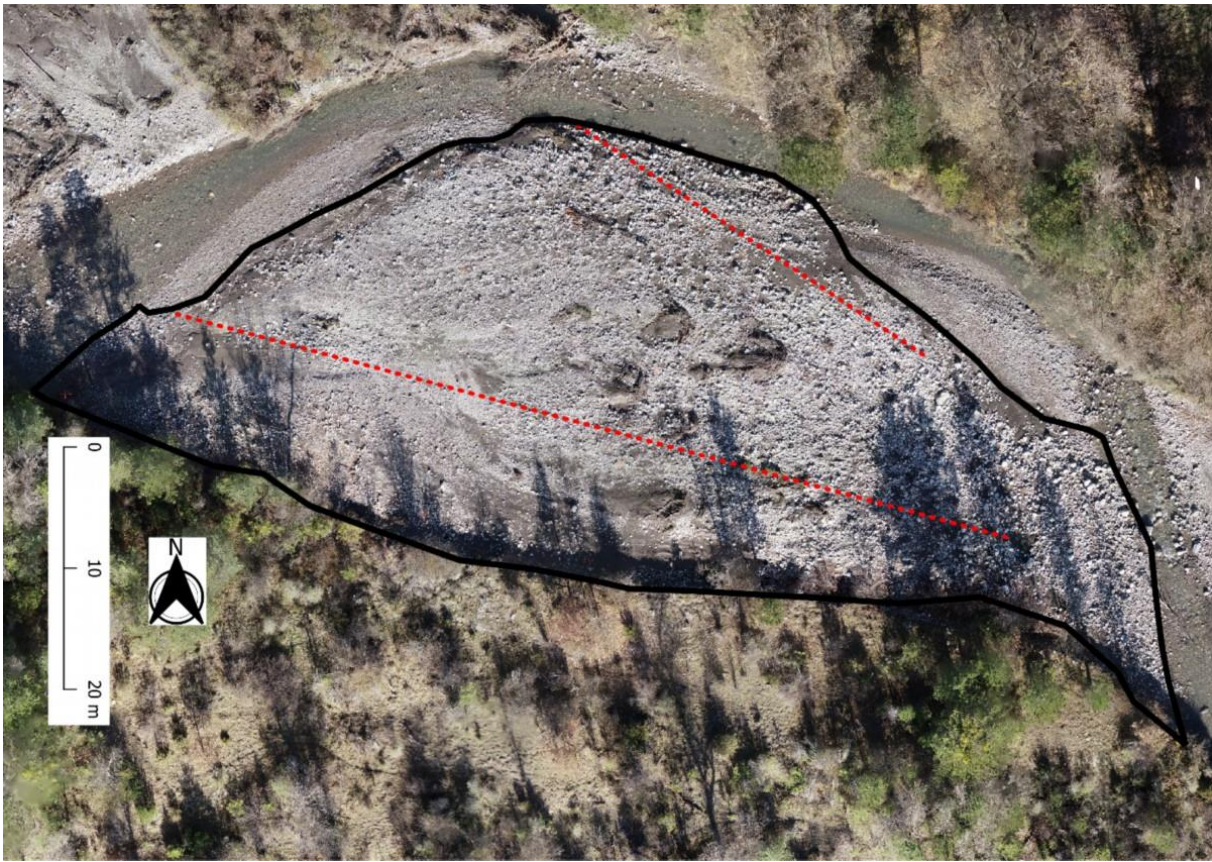


Figure S2: Sampling transects for the Wolman pebble counts of the Arigéol active channel. Note that the ortho-image is from 2021 and that the Wolman sampling was conducted in 2024. The distance between each transect is 100 m. Two particles were sampled every meter.



60 Figure S3: Sampling transects for the Wolman pebble counts of the bar of interest of the Bouinenc. Note that the ortho-image is from 2021 and that the Wolman sampling was conducted in 2024. Two particles were sampled every meter.

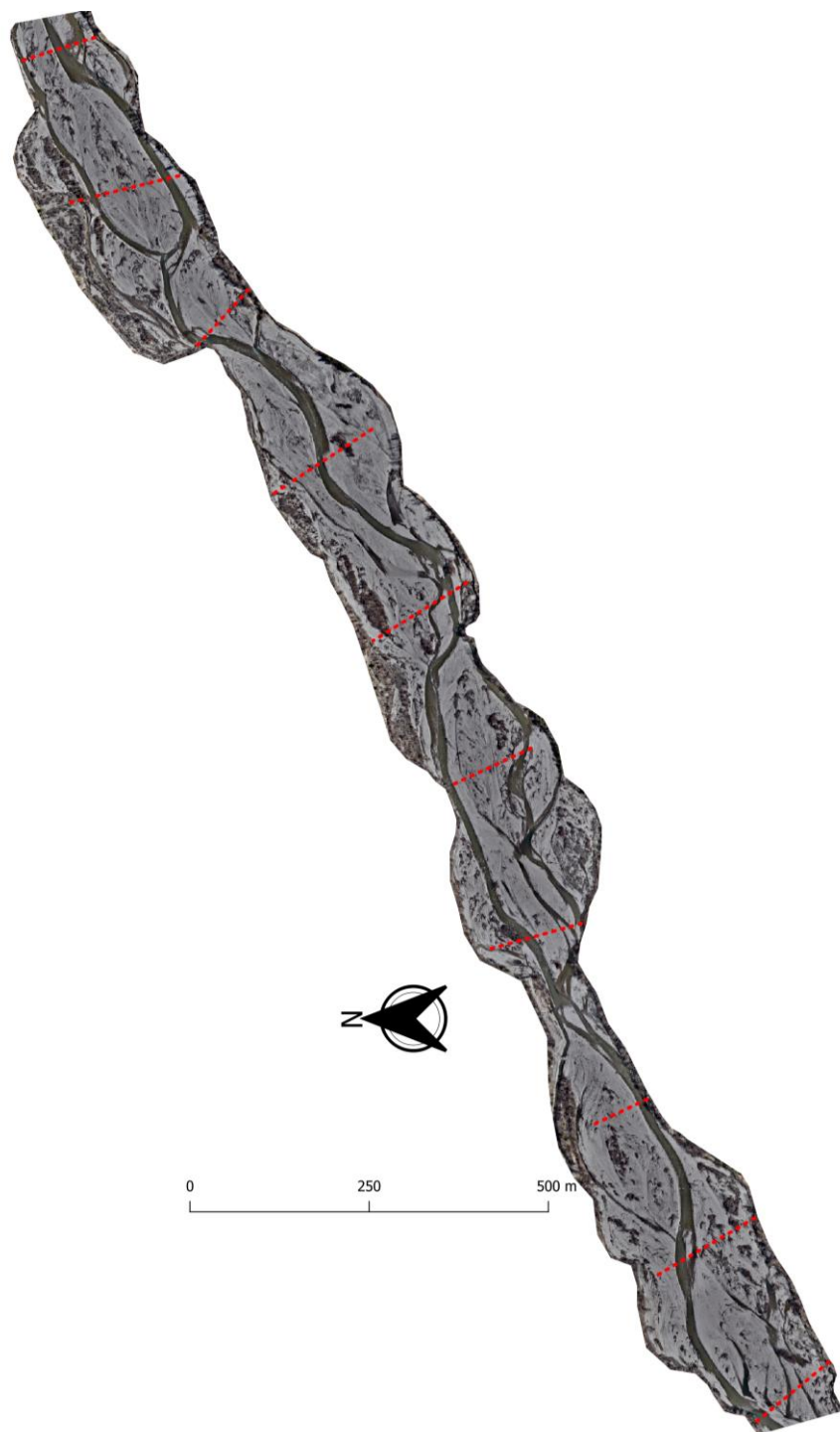
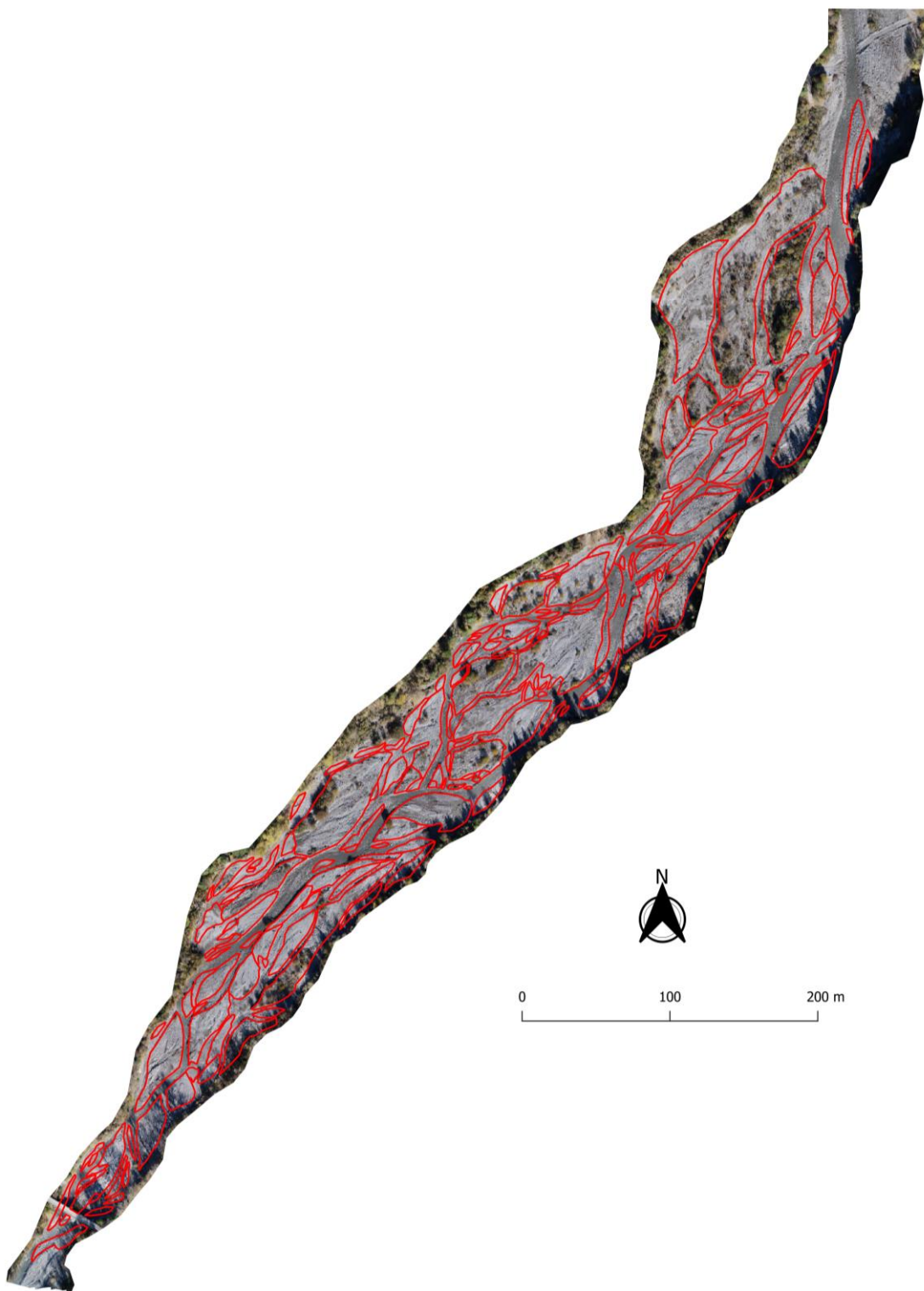


Figure S4 : Sampling transects for the Wolman pebble counts of the Drac active channel. Note that the ortho-image is from 2022 and that the Wolman sampling was conducted in 2024. The distance between each transect is 250 m. Two particles were sampled every two meters.



65 Figure S5: Manual digitizing of bars for the Arigéol



Arigéol sampling plot n°1



Arigéol sampling plot n°1



Arigéol sampling plot n°3



Arigéol sampling plot n°4



Arigéol sampling plot n°5



Arigéol sampling plot n°6



Arigéol sampling plot n°7



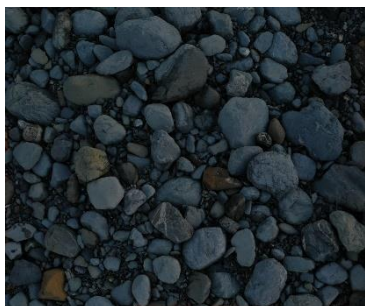
Arigéol sampling plot n°8



Arigéol sampling plot n°9



Arigéol sampling plot n°10



Arigéol sampling plot n°11



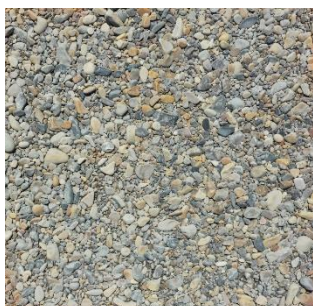
Asse sampling plot n°1



Asse sampling plot n°2



Asse sampling plot n°3



Asse sampling plot n°4



Asse sampling plot n°5



Asse sampling plot n°6



Asse sampling plot n°7



Asse sampling plot n°8



Asse sampling plot n°9



Asse sampling plot n°10



Béoux sampling plot n°1



Béoux sampling plot n°2



Béoux sampling plot n°3



Béoux sampling plot n°4



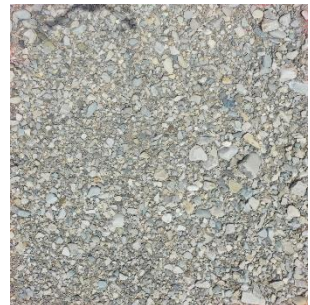
Béoux sampling plot n°5



Béoux sampling plot n°6



Béoux sampling plot n°7



Béoux sampling plot n°8



Béoux sampling plot n°9



Béoux sampling plot n°10



Bès sampling plot n°1



Bès sampling plot n°2



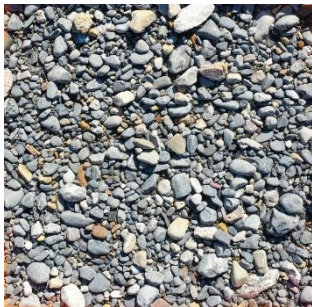
Bès sampling plot n°3



Bès sampling plot n°4



Bès sampling plot n°5



Bès sampling plot n°6



Bès sampling plot n°7



Bès sampling plot n°8



Bès sampling plot n°9



Bès sampling plot n°10



Bès sampling plot n°11



Bès sampling plot n°12



Bouinenc sampling plot n°1



Bouinenc sampling plot n°2



Bouinenc sampling plot n°3



Bouinenc sampling plot n°4



Bouinenc sampling plot n°5



Bouinenc sampling plot n°6



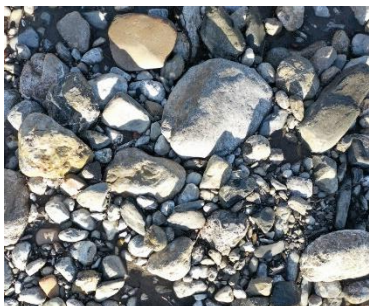
Bouinenc sampling plot n°7



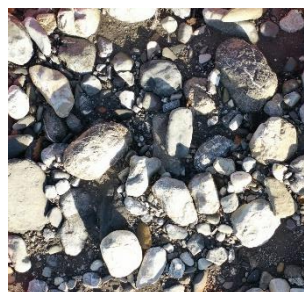
Bouinenc sampling plot n°8



Bouinenc sampling plot n°9



Bouinenc sampling plot n°10



Bouinenc sampling plot n°11



Drac sampling plot n°1



Drac sampling plot n°2



Drac sampling plot n°3



Drac sampling plot n°5



Drac sampling plot n°7



Drac sampling plot n°9



Drac sampling plot n°4



Drac sampling plot n°6



Drac sampling plot n°8



Drac sampling plot n°10



Drac sampling plot n°11



Drac sampling plot n°12



Drac sampling plot n°13



Drôme sampling plot n°1



Drôme sampling plot n°2



Drôme sampling plot n°3



Drôme sampling plot n°4



Drôme sampling plot n°5



Drôme sampling plot n°6



Drôme sampling plot n°7



Drôme sampling plot n°8



Drôme sampling plot n°9



Drôme sampling plot n°10



Drôme sampling plot n°11



Ebron sampling plot n°1



Ebron sampling plot n°2



Ebron sampling plot n°3



Ebron sampling plot n°4



Ebron sampling plot n°5



Ebron sampling plot n°6



Ebron sampling plot n°7



Ebron sampling plot n°8



Ebron sampling plot n°9



Ebron sampling plot n°10



Eygues sampling plot n°1



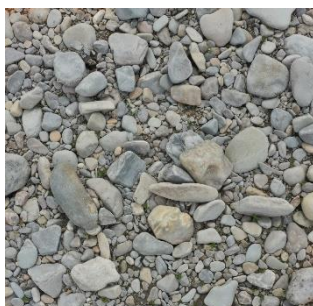
Eygues sampling plot n°2



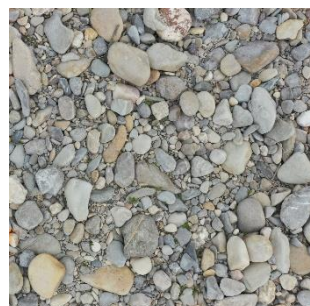
Eygues sampling plot n°3



Eygues sampling plot n°4



Eygues sampling plot n°5



Eygues sampling plot n°6



Eygues sampling plot n°7



Eygues sampling plot n°8



Eygues sampling plot n°9



Eygues sampling plot n°10



Eygues sampling plot n°11



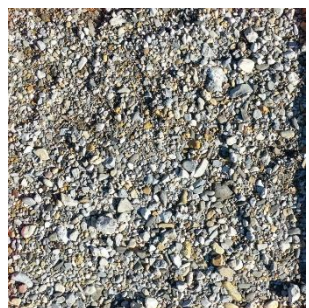
Galabre sampling plot n°1



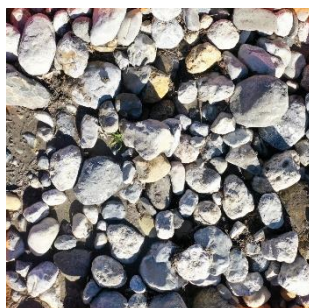
Galabre sampling plot n°2



Galabre sampling plot n°3



Galabre sampling plot n°4



Galabre sampling plot n°5



Galabre sampling plot n°6



Galabre sampling plot n°7



Galabre sampling plot n°8



Galabre sampling plot n°9



Galabre sampling plot n°10



Séveraisse sampling plot n°1



Séveraisse sampling plot n°2



Séveraisse sampling plot n°3



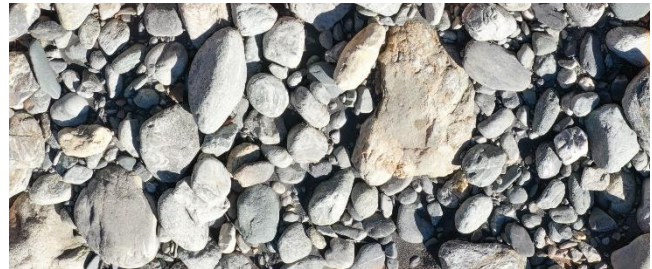
Séveraisse sampling plot n°4



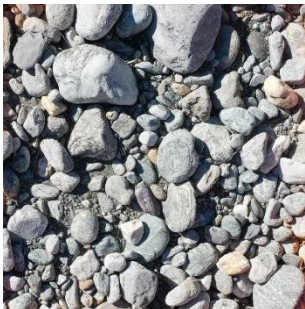
Séveraisse sampling plot n°5



Séveraisse sampling plot n°6



Séveraisse sampling plot n°7



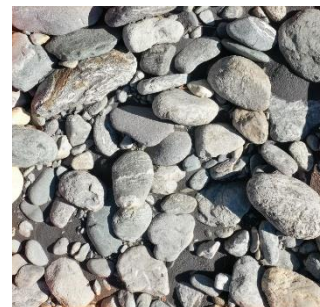
Séveraisse sampling plot n°8



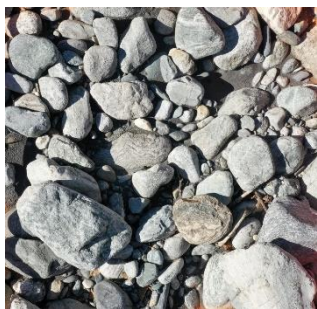
Séveraisse sampling plot n°9



Séveraisse sampling plot n°10



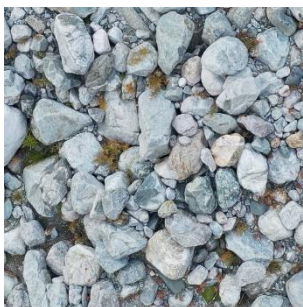
Séveraisse sampling plot n°11



Séveraisse sampling plot n°12



Séveraisse sampling plot n°13



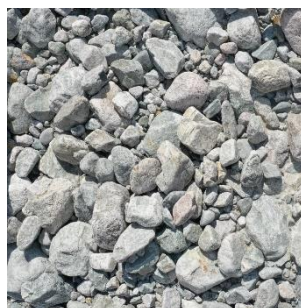
St-Pierre sampling plot n°1



St-Pierre sampling plot n°2



St-Pierre sampling plot n°3



St-Pierre sampling plot n°4



St-Pierre sampling plot n°5



St-Pierre sampling plot n°6



St-Pierre sampling plot n°7

Figure S6: Sampling plot photos



St-Pierre sampling plot n°8

References

- 70 Eltner, A., Kaiser, A., Castillo, C., Rock, G., Neugirg, F., and Abellán, A.: Image-based surface reconstruction in
geomorphometry – merits, limits and developments, *Earth Surf. Dyn.*, 4, 359–389, <https://doi.org/10.5194/esurf-4-359-2016>,
2016.
- James, M. R. and Robson, S.: Straightforward reconstruction of 3D surfaces and topography with a camera: Accuracy and
geoscience application: 3D SURFACES AND TOPOGRAPHY WITH A CAMERA, *J. Geophys. Res. Earth Surf.*, 117, n/a-
75 n/a, <https://doi.org/10.1029/2011JF002289>, 2012.
- Over, J.-S. R., Ritchie, A. C., Kranenburg, C. J., Brown, J. A., Buscombe, D., Noble, T., Sherwood, C. R., Warrick, J. A., et
Wernette, P. A.: Processing coastal imagery with Agisoft Metashape Professional Edition, version 1.6—Structure from
motion workflow documentation, U.S. Geological Survey, Reston, VA, 2021.